Graphene–Ti$_3$C$_2$T$_x$ MXene hybrid nanostructure: a promising material for sensitivity enhancement in plasmonic sensor

Ankit Kumar Pandey[1]

Abstract

MXene has emerged as a promising material for various optoelectronics applications. In view of the advanced properties of MXene, surface plasmon resonance (SPR)-based sensor utilising graphene–Ti$_3$C$_2$T$_x$ MXene hybrid nanostructure is proposed for sensitivity enhancement. The sensor's performance is theoretically demonstrated in terms of sensitivity and detection accuracy at incident light wavelength of 633 nm for a broad analyte refractive index (RI) range (1.33–1.36). Further, the effect of increasing Ti$_3$C$_2$T$_x$ MXene layers on the sensitivity is analysed. In addition, a significantly high average sensitivity is demonstrated at 532 nm for analyte RI in the vicinity of 1.32. This work will open new possibilities for graphene–Ti$_3$C$_2$T$_x$ MXene-based hybrid nanostructures in SPR-based bio- and gas-sensors.

Keywords Plasmonic sensor · 2D material · Sensitivity · Graphene · MXene · Hybrid nanostructure

1 Introduction

The integration of graphene-based system with modern technology has led towards its application in numerous optoelectronic devices [1]. The emergence of beyond graphene two-dimensional (2D) materials (e.g. phosphorene, transition metal dichalcogenides (TMDs), hexagonal boron nitrides, etc.) [2–5] has predicted their excellent integration. The quantum confinement has led to the advancement in the properties (chemical, physical and optical) of monolayer 2D materials from their bulk counterparts [2]. Moreover, the discovery of 2D Ti$_3$C$_2$T$_x$ in 2011 has open up new possibilities for its application [6]. It was assigned the name "MXene" due to its graphene-like morphology. The combination of the two imperative properties of metallic conductivity and hydrophilicity shown by MXene is one of the advantages over other 2D materials [7]. In addition, 2D structure of MXenes possesses a large surface area which makes them a promising material for application in electrochemical energy storage. Further, MXene-based device for wireless communication was reported by Sarycheva et al. [8]. Recently, Velusamy et al., demonstrated the first

plasmonic photodetector utilising Mo$_2$CT$_x$ MXene [9]. Apart from the discussed optoelectronics applications, MXene has witnessed its application in biomedical fields viz., bioimaging, biosensors, antibacterial and theranostics [10]. In the context of biosensors, surface plasmon resonance (SPR)-based sensors in particular, MXene is burgeoning as a promising material for performance enhancement of the detection scheme [11–13]. The transverse magnetic (TM) wave oscillations existing at metal–dielectric interfaces are usually referred as SPR [14]. The accurate sensing mechanism, ease of fabrication and low cost experimental arrangements have made SPR-based technique a preferable choice among other optical detection techniques [15].

The application of 2D materials for sensitivity enhancement in SPR sensors have been reported earlier [16–19]. In continuation, few layer 2D Ti$_3$C$_2$T$_x$ MXene in SPR-based sensors for sensitivity enhancement was reported by Wu et al. [11]. Significantly higher sensitivity values than conventional Au-based SPR sensor were reported at operating wavelengths of 633 and 532 nm. MXene-based ultrasensitive SPR biosensor has been reported recently for the detection of carcinoembryonic antigen with a detection limit of 0.07 fM [12]. Further, Xu et al. reported sensitivity enhancement using transition metal dichalcogenide (TMD) and Ti$_3$C$_2$T$_x$ MXene (with Au interlayer) layer with a high sensitivity value of 198°/RIU at 633 nm (analyte refractive index ~ 1.33) [13]. The effect of multilayer on the sensitivity

✉ Ankit Kumar Pandey
  ankitec1016@gmail.com; ankit.pandey@bennett.edu.in

1 Department of Electronics and Communication Engineering, Bennett University, Greater Noida, India

was also discussed. However, the width of SPR curve (i.e. FWHM—full width at half maximum) which gives crucial information about accuracy of detection and the optimization of metal layer thickness for minimum reflectance at resonance were not addressed. Moreover, there is need to explore the combination of graphene with 2D $Ti_3C_2T_x$ MXene in SPR-based sensor for a precise and high sensitive detection of biosamples.

The combination of graphene and $Ti_3C_2T_x$ MXene is the desirable one owing to their advanced properties. The electrical conductivity of graphene is higher than that of TMDs, which expedites the charge transfer among the layers. Furthermore, the graphene flakes can improve the mechanical strength of $Ti_3C_2T_x$ MXene after the formation of 2D heterostructure. Aïssa et al. reported the high conductivity property of 2D Ti_2CT_x MXene/graphene sandwich-like composite [20] which is the motivation behind this work. Recently, the hybrid combination of Ti_2CT_x MXene with reduced graphene oxide (rGO) has been reported for application in Li-ion storage [21]. Further, the hybrid film possesses several advantages such as, excellent cycling stability, rate performance and reversible capacity (700 mAh/g at 0.1 A/g). Zhao et al., proposed fabrication of 2D MXene/graphene heterostructure using Spray-assisted layer-by-layer (LbL) process [22]. Nevertheless, no prior works have been reported based on the application of graphene–MXene heterojunction/heterostructure in SPR-based sensors for performance enhancement. Previously, the incorporation of 2D materials with graphene layers has provided a path for sensitivity enhancement [17, 23]. Field enhancement at the interface [24] and increased surface adsorption in case of SPR-based sensors are the two main advantages of having heterostructure as analyte interacting layer. Thus, there are a lot of possibilities in exploring the sensing capabilities of graphene/MXene heterostructure.

Sensitivity enhancement of SPR-based sensors using graphene–$Ti_3C_2T_x$ MXene hybrid nanostructure is explored in this work based on the optimised metal thickness at two specific wavelengths (532 nm and 633 nm). These wavelengths are commonly used in the visible region for SPR-based sensing application. The optimization of metal thickness is performed to achieve minimum reflectance at resonance. In addition, the performance of the proposed sensor structure (SiO$_2$/Ag/ graphene/$Ti_3C_2T_x$ MXene) is also analysed in terms of detection accuracy (D.A). Further, the sensitivity enhancement with increasing the number of $Ti_3C_2T_x$ MXene monolayers is also demonstrated.
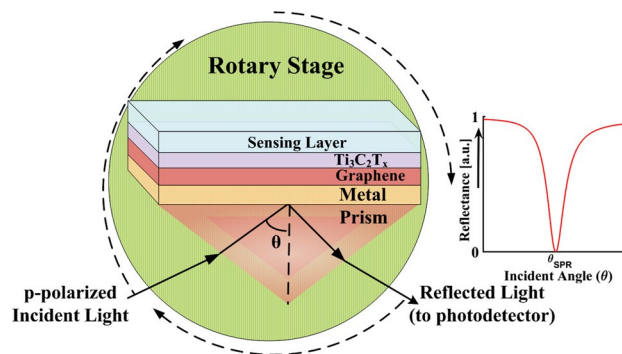
Fig. 1 Schematic of proposed Kretschmann configuration-based 5-layered SPR sensor using graphene monolayer–$Ti_3C_2T_x$ MXene. SPR curve experiences a narrow dip at θ_{SPR} when SPs are coupled with incident TM (transverse magnetic) light

2 Sensor's configuration and theoretical insights

The Kretschmann configuration-based sensor structure is shown in Fig. 1. During experimental realisation of such configurations, the main required components are laser source with polarizer, substrate/prism deposited with multi-layered structure and photodetector or charge coupled camera (CCD). The multi-layered structure is generally mounted on a rotary stage. Silica glass prism, i.e. SiO$_2$ (first layer) is considered as the coupling material. The second layer is SPR active metal silver (Ag). The third layer is graphene monolayer which is covered by $Ti_3C_2T_x$ MXene (fourth layer). This heterojunction (monolayer graphene and $Ti_3C_2T_x$ MXene) will also prevent Ag from possible oxidation concerns. The sensing layer is considered as the last layer.

In this work, the chosen dielectric constant values of different materials at λ = 633 nm and 532 nm are shown in Table 1. The reflectance (R) analysis is based on the variation of incident angle (i.e. angular interrogation method) at a fixed wavelength (here, λ = 633 nm or λ = 532 nm) of transverse magnetic (TM/ p-polarised) incident light. The numerical calculation of R is based the on N-layer transfer matrix method (TMM) [28]. Following equation represents coupling of incident light and SPs at metal–dielectric interface [14]:

$$\frac{\omega}{c} n_p \sin \theta_{SPR} = real\left(\frac{\omega}{c} \sqrt{\frac{\in_m \in_s}{\in_m + \in_s}} \right). \qquad (1)$$

Here, n_p is RI of the coupling prism, ω is the angular frequency of the incident light, c is the velocity of light in vacuum, ε_m and ε_s are the dielectric constant of the metal and sensing (analyte) layer, respectively. SPR curve experiences a narrow dip at a particular incident angle which is termed as the resonance angle (θ_{SPR}). A small change in ε_s value will lead towards the shifting in angular position of SPR dip.

## 3 Results and discussion

3.1 Metal layer thickness optimization

The minimum possible value of reflectance (R_{min}) at resonance can only be achieved by proper optimization of Ag layer thickness (t_{Ag}). This optimization plays a crucial role in strengthening of evanescent field. For optimization of t_{Ag}, $n_s = 1.333$ is taken into account for conventional Ag-based SPR sensor (without 2D material layer) and proposed structure. In case of conventional structure, R_{min} value of 1.5492×10^{-5} is calculated for $t_{Ag} = 55$ nm as shown in Fig. 2a. The optimised t_{Ag} value for proposed sensor is 41 nm at which $R_{min} = 4.9628 \times 10^{-4}$ as shown in Fig. 2b. These optimised t_{Ag} values are used in further numerical calculations.

Meanwhile, the R curves for conventional ($t_{Ag} = 55$ nm) and proposed sensor ($t_{Ag} = 41$ nm) are shown in Fig. 3 considering two different values of n_s (1.333 and 1.334). It is evident that $\Delta\theta_{SPR}$ (small change in the angular position of θ_{SPR}) for conventional and proposed sensor configurations are 0.167° (Fig. 3a) and 0.171° (Fig. 3b), respectively, for a small change in n_s value (i.e. $\Delta n_s = 0.001$). The sensitivity (S) which is an important performance parameter can be defined as $S = \Delta\theta_{SPR}/\Delta n_s$, generally expressed in deg./RIU. Thus, it can be inferred that the proposed sensor is able to provide higher sensitivity (0.171°/0.001 = 171°/RIU) as compared with that of conventional scheme (0.167°/0.001 = 167°/RIU). Moreover, Ag is the analyte interacting layer in conventional structure which may undergo some deterioration/degradation affecting the sensor's performance [29]. In the

Table 1 Dielectric constant values of layers at two different wavelengths used in this study

Layer	Dielectric constant at $\lambda = 633$ nm	Dielectric constant at $\lambda = 532$ nm
SiO$_2$ prism [25]	2.1228	2.1336
Ag [26]	$-18.295 + 0.48085i$	$-11.755 + 0.37038i$
Graphene (0.34 nm) [27]	$5.6167 + 7.4036i$	$5.6836 + 6.5522i$
Ti$_3$C$_2$T$_x$ MXene (0.993 nm) [11]	$3.8955 + 6.3308i$	$5.9696 + 5.280i$

Fig. 2 2D plot variation of *R* with t_{Ag} (in nm) and incident angle at $\lambda = 633$ nm with analyte RI = 1.333 for **a** conventional SPR-based sensor (Ag over prism) **b** proposed sensor configuration using monolayer Ti$_3$C$_2$T$_x$ MXene over monolayer graphene.
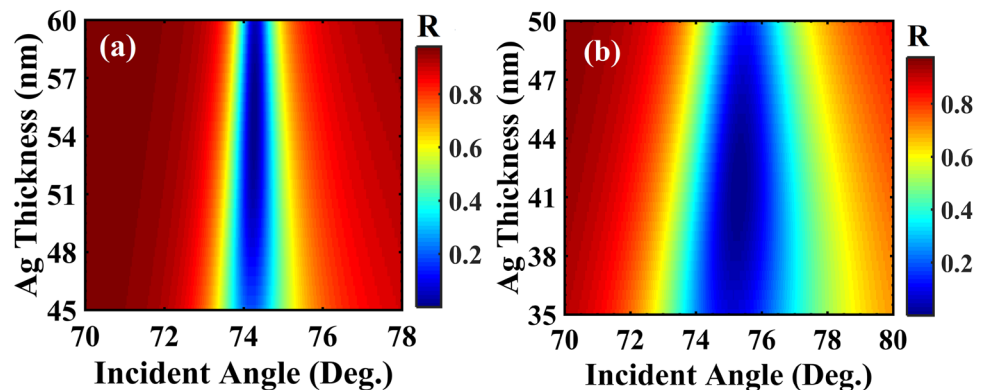
Fig. 3 Variation of reflectance with incident angle at $\lambda = 633$ nm for two different analyte RI in case of **a** conventional SPR-based sensor (Ag over prism) **b** proposed sensor configuration
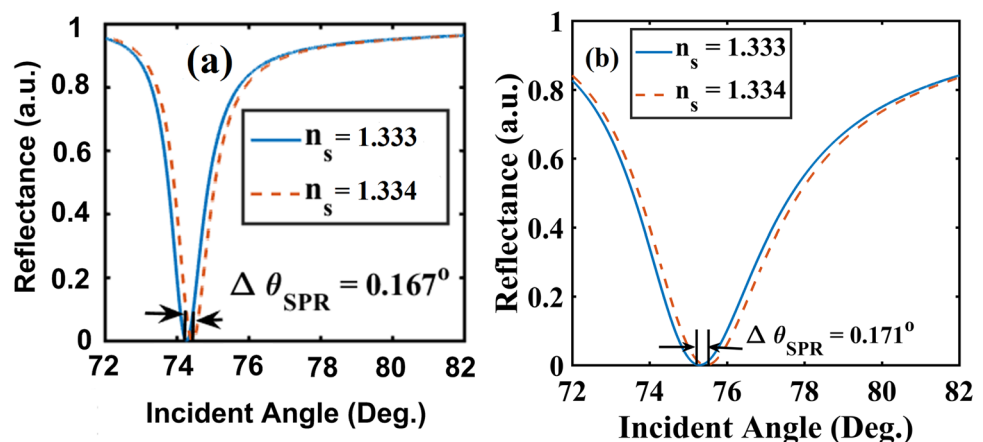
proposed structure, graphene–Ti$_3$C$_2$T$_x$ MXene heterojunction will act as a protective layer for Ag.

The variation of reflectance with incident angle for a range of analyte RI (1.33–1.36) is shown in Fig. 4a. The θ_{SPR} values of 74.786°, 76.530°, 78.50° and 80.821° are obtained for analyte RI values of 1.33, 1.34, 1.35 and 1.36, respectively. The shift in SPR curves for different analyte RI can be explained on the basis of Eq. (1). Further, to clearly visualise the variation of θ_{SPR} with analyte RI, Fig. 4b shows the 2D plot of the reflectance variation with analyte RI and incident angle. The occurrence of R_{min} will provide information about the angular position of θ_{SPR}. It is evident that θ_{SPR} increases when the analyte RI is increased.

To depict the performance of the sensor at $\lambda = 633$ nm, the variations of sensitivity and detection accuracy (D.A.) with analyte RI is shown in Fig. 5a. The D.A. can be defined as the reciprocal of FWHM (i.e. D.A. = 1/FWHM) [30]. Considering reference sample RI of 1.33, the sensitivity value increases from 169.60°/RIU to 201.166°/RIU for analyte RI of 1.335 and 1.360, respectively. However, the D.A. value decreases from 0.239 deg^{-1} to 0.185 deg^{-1} on increasing analyte RI from 1.335 to 1.360. Evidently, there is a trade-off between sensitivity and D.A. Thus, analyte RI range can be selected based on the requirements of high sensitivity and affordable D.A. value. Moreover, the effect of number of layers (L) of Ti$_3$C$_2$T$_x$ MXene over graphene on sensitivity is shown in Fig. 5b. For $n_s = 1.33$ and $\Delta n_s = 0.005$, the sensitivity increases form 169.60°/RIU ('$L=1$') to 196.86°/RIU ('$L=4$') which further decreases to 171.30°/RIU ('$L=6$'). In addition, for $n_s = 1.34$ and $\Delta n_s = 0.005$, a high sensitivity of 214.20 °/RIU is calculated at '$L=3$' which decreases to 145.00°/RIU ('$L=6$'). This decrease in sensitivity on increasing 'L' has been demonstrated earlier by Wu et al. [11] based on the movement of reflectance curve towards larger angle. This is due to the limitation in the range of incident angle from 0° to 90°. Thus, it can be interpreted that '$L=4$' at $\lambda = 633$ nm can be opted when the analyte RI is in the vicinity of 1.33 and 1.34.

The above discussion is meant for application of proposed SPR sensor at $\lambda = 633$ nm using monolayer graphene–Ti$_3$C$_2$T$_x$ MXene nanostructure. However, the analysis is also performed at commonly used wavelength of 532 nm in the visible region for SPR-based sensing application. Initially, the t_{Ag} value is optimised in view of R_{min} at resonance condition. Wavelength-dependent dielectric properties of the layers play an important role in optimising the Ag layer thickness at a particular wavelength. Considering

$n_s = 1.32$, $R_{min} = 2.2957 \times 10^{-4}$ is obtained at $t_{Ag} = 37$ nm ($\lambda = 532$ nm). Figure 6 a shows the variation of SPR curves with incident angle for different n_s (optimised $t_{Ag} = 37$ nm). The θ_{SPR} values for discrete n_s are 79.0° ($n_s = 1.32$), 80.156° ($n_s = 1.325$), 81.418° ($n_s = 1.33$) and 82.803° ($n_s = 1.335$). Thus, for a small Δn_s (1.335–1.32 = 0.015), the corresponding shift in angular position of resonance (i.e. $\Delta\theta_{SPR}$) is 3.803°. A significantly high average sensitivity of 253.533°/RIU (3.803°/0.015) along with a reasonable average FWHM value of 8.440° is calculated for the analyte RI in the vicinity of 1.32 and 1.33 in case of proposed SiO$_2$–Ag–graphene–Ti$_3$C$_2$T$_x$ MXene-based SPR sensor. In this context, the variation of $\Delta\theta_{SPR}$ with analyte RI (i.e. n_s) is shown in Fig. 6b. Further, when $n_s = 1.33$ and $\Delta n_s = 0.005$, a high sensitivity value of 277°/RIU (1.385°/0.005) is calculated. It should be noted that increasing n_s beyond 1.34 and (or) increasing 'L' will cause shift in the reflectance curve towards a greater angle (outside the range 0° to 90°). Thus, the monolayer MXene ($L=1$) over graphene is a preferable choice at 532 nm. Table 2 shows the sensitivity comparison among recently reported works and proposed work based on the SPR sensors utilising 2D Ti$_3$C$_2$T$_x$ MXene for sensitivity enhancement. Generally, a larger SPR shift is achieved in case of Au-based structure than that of Ag-based structure. In addition, the low RI substrate will be beneficial for achieving high sensitivity (due to large change in angle of reflection) which can be explained on the basis of Snell's law as reported in the previous study [31]. The proposed structure has the advantage of high sensitivity along with a reasonable detection accuracy.

4 Conclusion

SPR-based biosensor utilising graphene–Ti$_3$C$_2$T$_x$ MXene hybrid nanostructure is proposed in this work. The theoretical analysis is initiated with the optimization of Ag layer thickness. A sensitivity value of 169.60°/RIU (analyte RI ~ 1.33) is obtained for proposed sensor utilising monolayer graphene–Ti$_3$C$_2$T$_x$ MXene at incident light wavelength of 633 nm. Further, it is demonstrated that increasing Ti$_3$C$_2$T$_x$ MXene layers (L) over graphene enhances the sensitivity. On increasing the number of Ti$_3$C$_2$T$_x$ MXene layers, high sensitivity values of 196.86°/RIU ($L=4$) and 214.20°/RIU are ($L=3$) obtained at 633 nm for analyte RI values of 1.33 ($\Delta n_s = 0.005$) and 1.34 ($\Delta n_s = 0.005$), respectively. In addition, an average sensitivity and FWHM values of 253.533°/RIU and, 8.440°, respectively, are calculated at $\lambda = 532$ nm for analyte RI in the vicinity of 1.32. Thus, the proposed sensor configuration (SiO$_2$/Ag/graphene/Ti$_3$C$_2$T$_x$ MXene) is able to provide a high sensitivity with reasonable detection accuracy.

Fig. 4 Variation of reflectance with incident angle different analyte RI values (1.33–1.36) for proposed sensor at $\lambda = 633$ nm **a** SPR curves **b** 2D plot of the variation showing resonance angle (θ_{SPR}) shift on changing the analyte RI
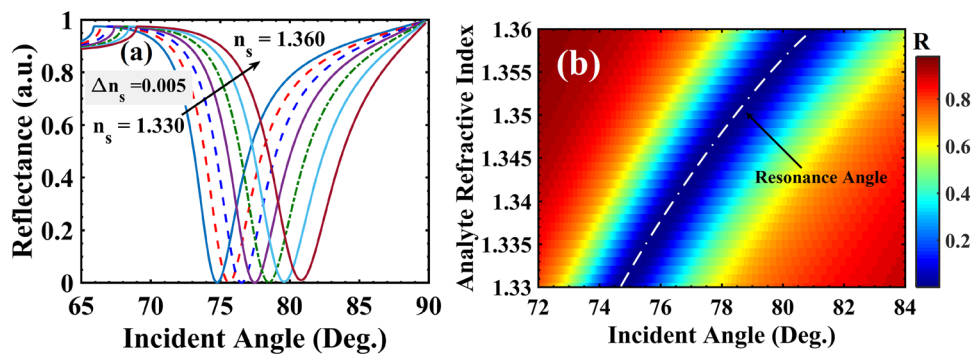
Fig. 5 a Variation of sensitivity and detection accuracy with analyte RI values (1.33–1.36) for proposed monolayer graphene–Ti$_3$C$_2$T$_x$ MXene sensor at $\lambda = 633$ nm **b** Sensitivity variation with number of MXene layer (L) over graphene monolayer for two different analyte RI values (1.33 and 1.34) and $\Delta n_s = 0.005$ at $\lambda = 633$ nm
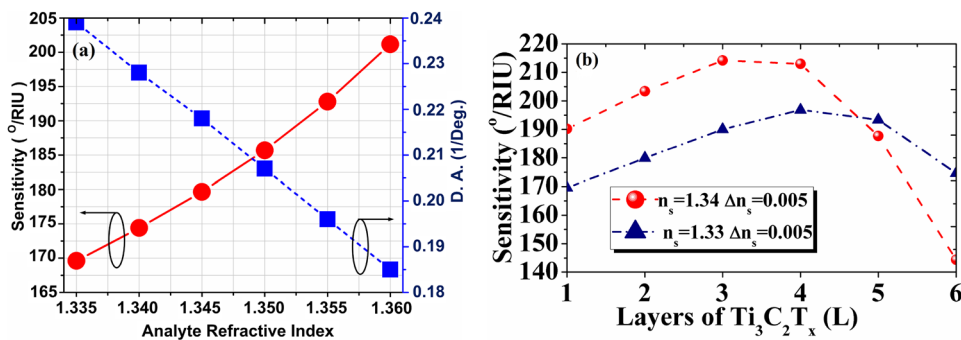
Fig. 6 a Variation of reflectance with incident angle different analyte RI values (1.320–1.335) for proposed sensor at $\lambda = 532$ nm (the monolayer graphene and monolayer Ti$_3$C$_2$T$_x$ MXene are used) **b** variation of $\Delta\theta_{SPR}$ with analyte refractive index at $\lambda = 532$ nm
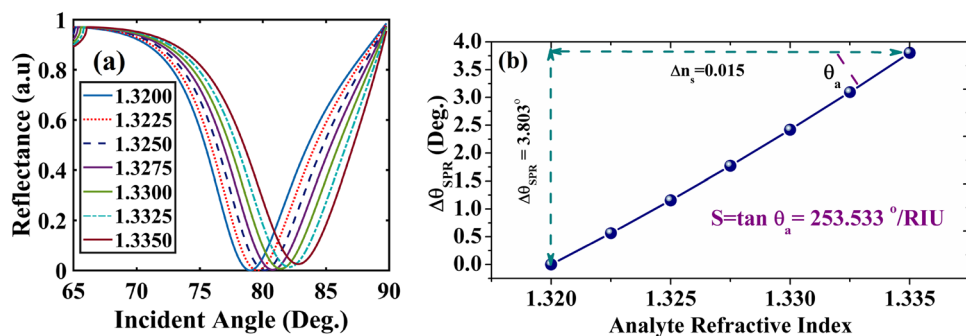
Table 2 Sensitivity comparison among recently reported works utilising 2D Ti$_3$C$_2$T$_x$ MXene

References	Modalities	λ (nm)	n_s and Δn_s	Sensitivity (^{o}/RIU)
Xu et al. [13]	BK7 + Au + TMD + Au + Ti$_3$C$_2$T$_x$	633	1.33, 0.005	198
Wu et al. [11]	BK7 + Au + Ti$_3$C$_2$T$_x$	633	1.33, 0.005	160
		532	1.325, 0.01	225.40
Srivastava et al. [32]	BK7 + Au + Ti$_3$C$_2$T$_x$ + WS$_2$ + BP	633	1.33, 0.005	190.22
This work	SiO$_2$ + Ag + graphene + Ti$_3$C$_2$T$_x$	633	1.33, 0.005	196.86
		532	1.32, 0.015	253.533
		532	1.33, 0.005	277.00

References

1. P. Avouris, M. Freitag, IEEE J. Sel. Top. Quantum Electron. **20**, 6000112 (2014)
2. G. Rubio-Bollinger, R. Guerrero, D. de Lara, J. Quereda, L. Vaquero-Garzon, N. Agraït, R. Bratschitsch, A. Castellanos-Gomez, Electronics **4**, 847 (2015)
3. M. Donarelli, L. Ottaviano, Sensors (Basel). **18**, (2018)
4. S. Balendhran, S. Walia, H. Nili, S. Sriram, M. Bhaskaran, Small **11**, 640 (2015)
5. Q. Peng, Z. Wang, B. Sa, B. Wu, Z. Sun, Sci. Rep. **6**, 31994 (2016)
6. M. Naguib, M. Kurtoglu, V. Presser, J. Lu, J. Niu, M. Heon, L. Hultman, Y. Gogotsi, M.W. Barsoum, Adv. Mater. **23**, 4248 (2011)
7. H. Kim, Z. Wang, H.N. Alshareef, Nano Energy **60**, 179 (2019)
8. A. Sarycheva, A. Polemi, Y. Liu, K. Dandekar, B. Anasori, Y. Gogotsi, Sci. Adv. **4**, 1 (2018)
9. D.B. Velusamy, J.K. El-Demellawi, A.M. El-Zohry, A. Giugni, S. Lopatin, M.N. Hedhili, A.E. Mansour, E. Di Fabrizio, O.F. Mohammed, H.N. Alshareef, Adv. Mater. **1807658**, 1 (2019)
10. K. Huang, Z. Li, J. Lin, G. Han, P. Huang, Chem. Soc. Rev. **47**, 5109 (2018)
11. L. Wu, Q. You, Y. Shan, S. Gan, Y. Zhao, X. Dai, Y. Xiang, Sensor. Actuat. B Chem. **277**, 210 (2018)
12. Q. Wu, N. Li, Y. Wang, Y. Liu, Y. Xu, S. Wei, J. Wu, J. Gia, X. Fang, F. Chen, X. Cui, Biosens. Bioelectron. **144**, 111697 (2019)
13. Y. Xu, Y.S. Ang, L. Wu, L.K. Ang, Nanomaterials **9**, 1 (2019)
14. H. Raether, *Surface Plasmons on Smooth and Rough Surfaces and on Gratings* (Springer-Verlag, New York, Berlin, Heidelberg, 1988).
15. J.-F. Masson, ACS Sens. **2**, 16 (2017)
16. A.K. Pandey, Photon. Nanostr. Fundam. Appl. **42**, 100863 (2020). https://doi.org/10.1016/j.photonics.2020.100863
17. L. Wu, J. Guo, Q. Wang, S. Lu, X. Dai, Y. Xiang, D. Fan, Sens. Actuat. B Chem. **249**, 542 (2017)
18. Z. Lin, L. Jiang, L. Wu, J. Guo, X. Dai, Y. Xiang, D. Fan, IEEE Photon. J. **8**, 1 (2016)
19. A.K. Sharma, A.K. Pandey, IEEE Photon. Technol. Lett. **30**, 595 (2018)
20. B. Aïssa, A. Ali, K.A. Mahmoud, T. Haddad, M. Nedil, Appl. Phys. Lett. **109**, 1 (2016)
21. S. Xu, Y. Dall'Agnese, J. Li, Y. Gogotsi, W. Han, Chem. Eur. J. **24**, 18556 (2018)
22. M.Q. Zhao, N. Trainor, C.E. Ren, M. Torelli, B. Anasori, Y. Gogotsi, Adv. Mater. Technol. **4**, 1 (2019)
23. L. Wu, J. Guo, X. Dai, Y. Xiang, D. Fan, Plasmonics 1 (2017)
24. A.K. Sharma, A.K. Pandey, B. Kaur, Materials (Basel). **12**, 1542 (2019)
25. I.H. Malitson, J. Opt. Soc. Am. **55**, 1205 (1965)
26. P.B. Johnson, R.W. Christy, Phys. Rev. B **6**, 4370 (1972)
27. J.W. Weber, V.E. Calado, M.C.M. van de Sanden, Appl. Phys. Lett. **97**, 130 (2010)
28. Q. Ouyang, S. Zeng, L. Jiang, L. Hong, G. Xu, X.Q. Dinh, J. Qian, S. He, J. Qu, P. Coquet, K.T. Yong, Sci. Rep. **6**, 1 (2016)
29. N.-H. Kim, M. Choi, T.W. Kim, W. Choi, S.Y. Park, K.M. Byun, Sensors **19**, 1894 (2019)
30. L. Wu, Z. Ling, L. Jiang, J. Guo, X. Dai, Y. Xiang, and D. Fan, IEEE Photonics J. **8**, (2016).
31. L. Wu, Y. Jia, L. Jiang, J. Guo, X. Dai, Y. Xiang, D. Fan, J. Light. Technol. **35**, 82 (2017)
32. A. Srivastava, A. Verma, R. Das, Y.K. Prajapati, Optik (Stuttg). **203**, 163430 (2020)